*Macromolecules* **2001,** *34,* 6461−6473

# Structure Factor of Semidilute Polymer Solution under Continuous Shear Flow: Numerical Analysis of a Two-Fluid Model and Comparison with Experiments

**Shin Saito, Mikihito Takenaka, Nobuyuki Toyoda, and Takeji Hashimoto***

*Department of Polymer Chemistry, Graduate School of Engineering, Kyoto University, Kyoto 606-8501, Japan*

*Received December 15, 2000; Revised Manuscript Received June 11, 2001*

ABSTRACT: We calculated the structure factor of a semidilute polymer solution under continuous shear flow using a theory first proposed by Helfand and Fredrickson which describes the dynamical coupling between stress and diffusion based on a two-fluid model. The Kaye−BKZ constitutive equation is applied to the stress term in the theory in order to express the non-Newtonian behavior, the normal stress effect, and the distribution of the stress relaxation. By taking account of the distribution of the stress relaxation, we can calculate the structure factor, in the context of a linearized dynamical equation, in the high shear rate regime $\dot{\gamma}\tau_m > 1$ with $\tau_m$ being the maximum relaxation time, at which the comparison between the theory and the experimental results is of greatest interest. Although the resulting structure factors show a qualitative agreement with experiments, some discrepancies exist such as the $\dot{\gamma}$ dependence of the peak position. We also examine the effect of normal stress on the structure factor and the value of $\dot{\gamma}$ at which the intensity diverges. The theoretical results are discussed in conjunction with experimental findings.

## 1. Introduction

A semidilute polymer solution in a single phase exhibits strong turbidity when subjected to shear flow. This phenomenon is called shear-induced enhancement of concentration fluctuations and/or phase separation and has been a fascinating subject of many experimental and theoretical studies over the past decade in the context of open, nonequilibrium, nonlinear phenomena. This phenomenon is one of the most remarkable properties of a semidilute polymer solution and is attributed to so-called "dynamical coupling between stress and diffusion": the local variation of the composition generates the local stress, and the built-up stress influences the spatial inhomogeneity of the composition. Under shear flow, the local stress tends to become higher in the region having higher polymer concentration: the local stress built-up tends to be relaxed, which results in the "solvent squeezing" from this region and hence the enhancement of the concentration fluctuations.

Experimentally, the enhancement of concentration fluctuations by shear flow has been observed by light scattering (LS)[1−5] and small-angle neutron scattering (SANS).[4−7] When the shear rate $\dot{\gamma}$ is larger than a critical value, the shear-enhanced scattering intensity has appeared in the first and third quadrants of the $q_x$−$q_y$ plane even in the case where $\dot{\gamma}$ is smaller than the longest relaxation rate $\tau_m^{-1}$ of the solution, as observed by Wu et al. with LS.[1] However in the $q_x$−$q_z$ plane the enhanced scattering has not been obtained, as found by us with LS and SANS.[2,3,5] Here $q$ is the magnitude of the scattering wave vector defined as $q = |\mathbf{q}| = (4\pi/\lambda)\sin(\theta/2)$, where $\lambda$ is the wavelength of the incident beam and $\theta$ the scattering angle in medium. $x$, $y$, and $z$ indicate respectively the flow direction, the velocity gradient direction, and the neutral direction, and $q_x$, $q_y$, and $q_z$ are the respective components of $\mathbf{q}$. In the case when $\dot{\gamma}$ is larger than $\tau_m^{-1}$, not only in the $q_x$−$q_y$ plane but also in the $q_x$−$q_z$ plane the enhanced scattering has been observed by LS and SANS.[5]

In theoretical studies, a dynamical equation for the concentration fluctuations, which accounts for the dynamical coupling between stress and diffusion, has been proposed by Helfand and Fredrickson,[8] Milner,[9] and Onuki[10] (HFMO). Milner[9] calculated the structure factor by using this equation coupled with rheological constitutive equations, in which both the amplitude of the concentration fluctuations and the viscoelastic responses were linearized, respectively, with respect to the concentration fluctuations and the shear rate, while Ji and Helfand[11] only linearized the amplitude of the concentration fluctuations. The shape of these structure factors were found to agree with the observed scattering intensity distribution qualitatively,[1] indicating that the theory can describe the enhancement of concentration fluctuations under shear flow. However, most calculations of the structure factor and the comparisons with experimental results have been limited to the $\dot{\gamma}$ region satisfying $\dot{\gamma}\tau_m^{-1} \equiv W_i$ (Weisenberg number) $\lesssim 1$, since they have employed a single stress relaxation process for the constitutive equation.[9,11] The shear stress, hence, has a maximum at $W_i = 1$, which is inconsistent with the realistic behavior where shear stress increases monotonically with $W_i$. This means that our experimental results in the $q_x$−$q_z$ plane at $W_i \gtrsim 1$ cannot be compared with the previous theoretical calculation.

In this paper, to compare the theory and our experimental results in the $q_x$−$q_z$ plane and at $W_i \gtrsim 1$ where our system shows a remarkable shear-thinning and hence non-Newtonian behaviors, we present a theoretical analysis of the structure factor and viscoelastic behaviors based on a time-dependent Ginzburg−Landau type of dynamical equation based on a theory proposed by HFMO. For this purpose, we employed the constitutive equation proposed by Kaye−Bernstein−Kearsley−Zapas (Kaye−BKZ),[12,13] which accounts for the non-

---

* To whom correspondence should be addressed.

10.1021/ma0021390 CCC: $20.00

Newtonian behavior, the normal stress effect, and the distribution of the stress relaxation, for the stress terms in the HFMO dynamical equation. By including the distribution of the stress relaxation, the shear stress and the first normal stress difference can be described more precisely even at $W_i \gtrsim 1$, and the experimental structure factor measured under this condition can be compared with the theoretical structure factor.

## 2. Theory

**2.1. Dynamical Coupling between Stress and Diffusion.** In a semidilute polymer solution, the stress and the diffusion of solvents and polymers are coupled. This arises from asymmetry in the relative motion of the polymer and the solvent ("dynamical asymmetry"). To illustrate this situation, the theorists employed a two-fluid model of polymer solution[14] and established dynamical equations of the concentration fluctuations. Here, we introduce a theoretical scheme proposed by Onuki[10] and derive a equation of a steady-state structure factor within the linear approximation.

According to the HFMO theory, the dynamical equation of the concentration fluctuations which accounts for the dynamical stress–diffusion coupling is as follows:

$$\left(\frac{\partial}{\partial t} + \mathbf{v}\cdot\nabla\right)\phi = \nabla\cdot L\left[\nabla\frac{\delta F}{\delta\phi} - \frac{1}{\phi}\nabla\cdot\boldsymbol{\sigma}^{(n)}\right] \tag{1}$$

where $\mathbf{v}$ is the average velocity of the polymer and the solvent defined by eq 2, $\phi$ the volume fraction of polymer, $L$ the Onsager coefficient, $F$ the free energy functional, and $\boldsymbol{\sigma}^{(n)}$ the network stress tensor.

$$\mathbf{v} = \frac{1}{\rho}(\rho_{\mathrm{p}}\mathbf{v}_{\mathrm{p}} + \rho_{\mathrm{s}}\mathbf{v}_{\mathrm{s}}) \tag{2}$$

In eq 2 $\rho_{\mathrm{p}}$ and $\rho_{\mathrm{s}}$ are the mass densities of the polymer and the solvent, $\mathbf{v}_{\mathrm{p}}$ and $\mathbf{v}_{\mathrm{s}}$ are the velocities of the polymer and the solvent, and $\rho$ is the total density, $\rho = \rho_{\mathrm{p}} + \rho_{\mathrm{s}}$. In eq 1, the thermal noise term, which is not needed for the derivation of the relaxation rate of the concentration fluctuations below (eq 4) but is needed for the derivation of the equation of the steady-state structure factor (eq 5), is neglected. In the two fluid model, $\boldsymbol{\sigma}^{(n)}$ differs from the mechanical tensor $\boldsymbol{\sigma}$ by the isotropic tensor, $(\pi + p)\mathbf{I}$,[15] where $\pi$ is the osmotic pressure and $p$ the hydrostatic pressure. On the assumption that Tr $\boldsymbol{\sigma}^{(n)}$ is zero,[15] we have

$$\boldsymbol{\sigma}^{(n)} = \boldsymbol{\sigma} - \frac{1}{3}(\mathrm{Tr}\ \boldsymbol{\sigma})I \tag{3}$$

The above type of equation was first derived by Helfand and Fredrickson[8] for sheared polymer solution. Equation 1 implies that the imbalance of the network stress ($\nabla\cdot\boldsymbol{\sigma}^{(n)} \neq 0$) gives rise to the relative motion of the polymer and the solvent.

Calculation of the stress term $\nabla\cdot\nabla\cdot\boldsymbol{\sigma}^{(n)}$ in eq 1 by incorporating both the shear stress $\sigma_{xy}$ and the first normal stress difference $N_1$, linearization with respect to $\phi$, and the Fourier transform of eq 1 give the following relaxation rate of the concentration fluctuations:

$$\Gamma(\mathbf{q}) = L\left\{q^2(r_0 + Cq^2) - \frac{1}{\phi}\left[2q_xq_y\left(\frac{\partial\sigma_{xy}}{\partial\phi}\right) + \frac{1}{3}(2q_x^{\ 2} - q_y^{\ 2} - q_z^{\ 2})\left(\frac{\partial N_1}{\partial\phi}\right)\right]\right\} \tag{4}$$

The details of the calculation is given in the Appendix. This equation indicates that the stress terms (inside the brackets) slow down the relaxation rate of the concentration fluctuations, compared to the quiescent state (stress terms are zero). Taking into account the convection by shear flow, the steady-state structure factor becomes the following form:[17,18]

$$I(\mathbf{q}) = \int_0^\infty \mathrm{d}s\ 2L|\mathbf{k}(s)|^2 \exp[-2\int_0^s \mathrm{d}t\ \Gamma(\mathbf{k}(t))] \tag{5}$$

with

$$\mathbf{k}(t) = \mathbf{q} + \dot{\gamma}tq_x\mathbf{e}_y \tag{6}$$

By substituting eq 6 into eq 4, and also eq 4 into eq 5, we can obtain $I(\mathbf{q})$ in the integral form. Thus, the contribution of $\sigma_{xy}$ and $N_1$ to the relaxation rate (eq 4) and hence the scattering intensity (eq 5) are explicitly incorporated. Limitations and applicability of the theory will be separately discussed later in section 4.1.

Here, let us look at the details of $\Gamma(\mathbf{q})$. Obviously, incorporating the convective effect (eq 6) into eq 4 makes $\Gamma(\mathbf{q})$ time dependent. We shall first concentrate on the effect of shear stress on $\Gamma(\mathbf{q})$. From eq 4, without convection, $2q_xq_y(\partial\sigma_{xy}/\partial\phi)$ is positive in the first and third quadrants of the $q_x$–$q_y$ plane ($q_xq_y > 0$) and negative in the second and fourth quadrants of the $q_x$–$q_y$ plane ($q_xq_y < 0$). Therefore, the shear stress tends to enhance the fluctuations in the first and third quadrants and tends to suppress those in the second and fourth quadrants. In the $q_x$–$q_z$ plane, the effect of the shear stress vanishes since $q_y = 0$. These trends, however, are altered by incorporating the convective effect, changing the coefficient of the shear stress, $2q_xq_y$, into $2(q_xq_y + \dot{\gamma}tq_x^2)$. In this case, this coefficient is always positive in the first and third quadrants in the $q_x$–$q_y$ plane and all over the $q_x$–$q_z$ plane (since $q_y = 0$) and hence tends to enhance the concentration fluctuations in these $q$ regions. In the second and fourth quadrants in the $q_x$–$q_y$ plane, on the other hand, this coefficient is negative and positive before and after $t = -q_y/\dot{\gamma}q_x$, respectively, and hence the shear stress tends to suppress and enhance the concentration fluctuations before and after $t = -q_y/\dot{\gamma}q_x$, respectively.

Next we shall consider the effect of $N_1$. From eq 4, without the convective effect, the coefficient for $N_1$, $(2q_x^2 - q_y^2 - q_z^2)/3$, is positive along $q_x$ ($q_y = q_z = 0$) and negative along $q_y$ ($q_x = q_z = 0$) and $q_z$ ($q_x = q_y = 0$), and hence $N_1$ tends to enhance the fluctuations along $q_x$ and tends to suppress those along $q_y$ and $q_z$. However, these trends are changed by taking the convective effect into account, giving the coefficient $^1/_3[(2 - \dot{\gamma}^2t^2)q_x^2 - q_y^2 - q_z^2 - 2\dot{\gamma}tq_xq_y]$. Thus, the trend along $q_x$ becomes complicated, while those along $q_y$ and $q_z$ are unchanged. The coefficient along $q_x$, proportional to $(2 - \dot{\gamma}^2t^2)$, is positive and negative before and after $\dot{\gamma}t = \sqrt{2}$, respectively, indicating that the fluctuations along $q_x$ tend to be enhanced and suppressed before and after $\dot{\gamma}t = \sqrt{2}$, respectively. Whether the coefficient for $N_1$ is positive or negative in the $q_x$–$q_y$ plane is quite complicated, since the cross term $-2\dot{\gamma}tq_xq_y$ exists. We do not touch on the details to avoid confusion. We can say that this coefficient becomes negative at a sufficiently long time, revealing that $N_1$ tends to suppress the concentration fluctuations in the $q_x$–$q_y$ plane at the sufficiently long time.

For the numerical evaluation of eq 5, the actual forms of the stress terms, i.e., $\partial\sigma_{xy}/\partial\phi$ and $\partial N_1/\partial\phi$, are needed. In this paper, those are given by the simplest version of a Kaye–BKZ equation as described in the following section. A set of parameters required for numerical analyses of the theory will be described later in section 3.1.

**2.2. Kaye–BKZ Equation.** A constitutive equation represents a general relation between stress and strain (or strain rate). The Kaye–BKZ equation is one of the integral constitutive equation developed independently by Kaye[12] and by Bernstein, Kearsley, and Zapas.[13] Laun[21] has calculated the shear stress $\sigma_{xy}(t)$ and the first normal stress difference $N_1(t)$ by using the simplest version of the Kaye–BKZ equation. Using a damping function $h(r) \equiv G(t;\gamma)/G(t;0) = \exp(-n\gamma)$[20] with $G(t;\gamma)$ and $G(t;0)$ being the relaxation modulus obtained for the step strain $\gamma$ and for the extrapolated step strain $\gamma \to 0$, respectively, and $n$ being the nonlinearity parameter for $G(t;\gamma)$, $\sigma_{xy}(t)$ and $N_1(t)$ are given by

$$\sigma_{xy}(t) = \dot{\gamma}\sum_i \frac{G_i}{\tau_i K_1^{\,2}}[1 - (1 - n\dot{\gamma}\tau_i K_1 t)\exp(-K_1 t)] \quad (7)$$

$$N_1(t) = 2\dot{\gamma}^2 \sum_i \frac{G_i}{\tau_i K_1^{\,3}}\left[1 - \left(1 + K_1 t - \frac{n\dot{\gamma}\tau_i}{2}K_1^{\,2}t^2\right)\exp(-K_1 t)\right] \quad (8)$$

where $G_i$ and $\tau_i$ are respectively the relaxation modulus and the relaxation time of $i$th mode, and $K_1 = \tau_i^{-1} + n\dot{\gamma}$. In eq 4, the derivatives of $\sigma_{xy}$ and $N_1$ with respect to $\phi$ are needed. In the semidilute regime, $\tau_i$ and $G_i$ obey the following power law:

$$G_i = G_{0i}\phi^{\alpha} \quad (9)$$

$$\tau_i = \tau_{0i}\phi^{\beta} \quad (10)$$

where it is assumed that the $\phi$ dependence of $G_i$ and $\tau_i$ is independent of $i$.[22] This indicates that $\sigma_{xy}$ and $N_1$ depend on $\phi$ through the $\phi$ dependence of $G_i$ and $\tau_i$. Then the derivatives become

$$\frac{\partial\sigma_{xy}}{\partial\phi} = \dot{\gamma}\phi^{\alpha-\beta-1}\sum_i \frac{G_{0i}}{\tau_{0i}K_2^{\,2}}\left\{\frac{2\beta\phi^{-\beta}}{\tau_{0i}K_2} + [\alpha - \beta + n\dot{\gamma}\beta t(\tau_{0i}\phi^{\beta}K_2 - 1)]\exp(-K_2 t) - \left[\alpha - \beta + \frac{\beta\phi^{-\beta}}{\tau_{0i}}\left(\frac{2}{K_2} - t\right)\right](1 - n\dot{\gamma}\tau_{0i}\phi^{\beta}K_2 t)\exp(-K_2 t)\right\} \quad (11)$$

$$\frac{\partial N_1}{\partial\phi} = 2\dot{\gamma}^2\phi^{\alpha-\beta-1}\sum_i \frac{G_{0i}}{\tau_{0i}K_2^{\,3}}\left\{\alpha - \beta + \frac{3\beta\phi^{-\beta}}{\tau_{0i}K_2} - \left[\alpha - \beta + \frac{\beta\phi^{-\beta}}{\tau_{0i}}\left(\frac{3}{K_2} + t\right)\right]K_3\exp(-K_2 t) + \left[\frac{\phi^{-\beta}t}{\tau_{0i}} + n\dot{\gamma}t^2 K_2\left(\frac{1}{2}\tau_{0i}\phi^{\beta}K_2 - 1\right)\right]\beta\exp(-K_2 t)\right\} \quad (12)$$

where

$$K_2 = \tau_{0i}^{\ -1}\phi^{-\beta} + n\dot{\gamma} \quad (13)$$

$$K_3 = 1 + K_2 t - \frac{1}{2}n\dot{\gamma}\tau_{0i}\phi^{\beta}K_2^{\,2}t^2 \quad (14)$$

**Table 1. Characteristics of the Polymer Solutions Used in This Work**

| | $M_w$ | $M_w/M_n$ | $c$ [wt %] | $c/c^*$ | $T_{cl}$ [°C][a] | $\tau_m$ [s][b] |
|---|---|---|---|---|---|---|
| solution A | $5.48 \times 10^6$ | 1.15 | 6.0 | 6.4 | 13.8 | 37.7 (25.0 °C) |
| solution B | $2.89 \times 10^6$ | 1.09 | 4.0 | 3.1 | 14.2 | 42.9 (15.0 °C) |
| solution C[c] | $2.00 \times 10^6$ | | 8.0 | 6.4 | | 103 (9.0 °C) |

[a] Cloud point. [b] Maximum relaxation time obtained from the steady-shear viscosity measurement. [c] Deuterated polystyrene.

## 3. Numerical Analysis

**3.1. Parameters.** To compute eqs 4 and 5 numerically, appropriate values should be chosen for parameters ($\tau_i$, $G_i$, $\alpha$, $\beta$, $r_0$, $C$, $L$). In this paper, we use the rheological parameters (relaxation moduli, relaxation times) experimentally measured for a polystyrene/dioctyl phthalate solution on our own. An appropriate ratio of the plateau modulus to the osmotic modulus is used as a reference to determine the thermodynamic parameter ($r_0$).[9]

**3.1.1. Rheological Parameters.** To obtain the rheological parameters ($\tau_i$, $G_i$), the stress relaxation experiment was conducted on a semidilute polystyrene (PS) solution in dioctyl phthalate (DOP) (solution A). PS has a weight-average molecular weight of $5.48 \times 10^6$ and the polydispersity index of 1.15. The concentration is 6.0 wt %, which is 6.4 times as concentrated as the overlap concentration. The characteristic of the solution is summarized in Table 1, in which $M_w$, $M_w/M_n$, concentration ($c$), $c/c^*$ with $c^*$ being the overlap concentration, the cloud point $T_{cl}$, and the maximum relaxation time $\tau_m$ are presented. The measurement was carried out with ARES-FS (Rheometrics Scientific Co. Ltd.) with a cone–plate geometry.

Figure 1 shows the stress relaxation modulus $G(t)$ (circles) for solution A after imposing a step strain of 0.5 at 25 °C. From these data, we extracted the discrete relaxation spectrum using procedure X.[29] The eight relaxation modes were found as listed in Table 2. In Figure 1, the relaxation modulus is reproduced (dotted line) with $G(t) = \sum_{i=0}^{7} G_i \exp(-t/\tau_i)$, showing a good agreement with the experimental data at $t < 100$. At $t > 100$, the nonrelaxation contribution (i.e., an apparatus error) causes some discrepancy between them.

To check the behavior of the viscoelastic functions calculated from the Kaye–BKZ equation using above relaxation spectra, $\eta$, $\sigma_{xy}$, and $N_1$ as a function of $\dot{\gamma}$ are shown in Figure 2 (solid lines), where the data measured for solution A by the steady shear experiment are also included. (The experimental data on $N_1$ are not available for this solution.) In the Kaye–BKZ equation, the nonlinear parameter $n$ plays an important role to control the shape of the rheological functions. This parameter $n$ should be determined by the stress relaxation experiment for various $\gamma$.[20] In this paper, however, we use $n$ as an adjustable parameter obtained by fitting the shape of the calculated rheological functions to those obtained experimentally. Although the level of $\eta$ and $\sigma_{xy}$ calculated slightly differs from the experimental data (Figure

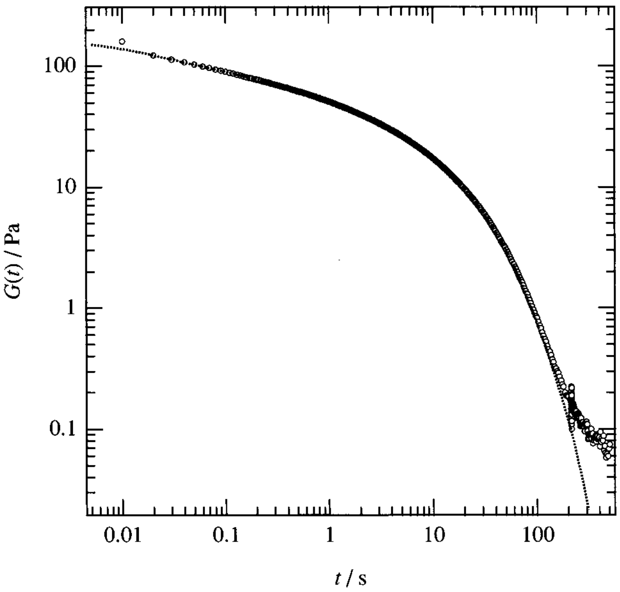

**Figure 1.** Relaxation modulus for solution A after a step strain of 0.5 at 25 °C. The circles denote the experimental data for solution A, and the dotted line denotes $G(t) = \sum_{i=0}^{7} G_i \exp(-t/\tau_i)$ using the discrete relaxation spectra given in Table 2.

**Table 2. Discrete Relaxation Spectra Obtained from *G*(*t*) for Solution A**

| mode | $G_i$ [Pa] | $\tau_i$ [s] | mode | $G_i$ [Pa] | $\tau_i$ [s] |
|---|---|---|---|---|---|
| 0 | 2.16 | 67.7 | 4 | 20.3 | 0.650 |
| 1 | 15.1 | 24.4 | 5 | 19.3 | 0.198 |
| 2 | 18.8 | 7.59 | 6 | 28.1 | 0.0582 |
| 3 | 20.7 | 2.27 | 7 | 41.4 | 0.0135 |

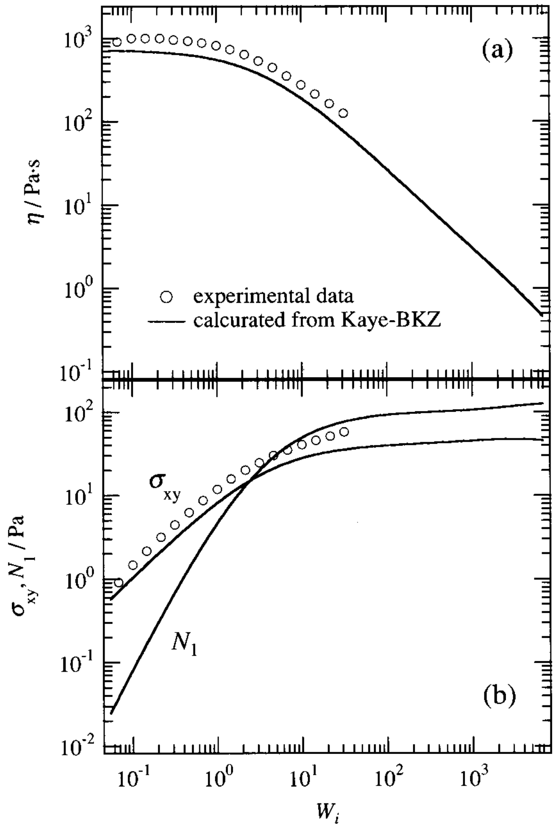

**Figure 2.** (a) Steady shear viscosity $\eta$ as a function of $W_i \equiv \dot{\gamma}\tau_m$ obtained by the experiment for solution A (open circles) and calculated by the Kaye−BKZ equation with $n = 0.4$ (solid line). (b) Shear stress and the first normal stress difference as a function of $W_i$ calculated by the Kaye−BKZ equation with $n = 0.4$ (solid lines). The open circles denote the shear stress obtained by the experiment for solution A.

**Table 3. Parameters Used at *r* = 0.93**

| $\phi$ | $r_0$ [Pa] | $C$ [Pa nm$^2$] | $\xi$ [nm] |
|---|---|---|---|
| $5.68 \times 10^{-2}$ | $5.5 \times 10^4$ | $5.5 \times 10^6$ | 10 |

2), the shapes of two data become almost identical for $n = 0.4$. Therefore, we employ $n = 0.4$ hereafter.

Next the values of $\alpha$ and $\beta$ in eqs 9 and 10 should be concerned. According to Adam and Delsanti,[27] the shear modulus and the maximum relaxation time of a semidilute solution in Θ condition (polystyrene in cyclohexane) are given as a function of $\phi$ as $G \sim \phi^{\alpha} = \phi^{2.3}$ and $\tau \sim \phi^{\beta} = \phi^{2.8}$. On the assumption that the exponents hold irrespective of the solvent species near the Θ condition, we thus adopted $\alpha = 2.3$ and $\beta = 2.8$.

**3.1.2. Thermodynamic Parameters.** To determine the thermodynamic parameters ($r_0$, $C$, $L$), we introduce a ratio of the plateau modulus to the osmotic modulus $r \equiv G_N/K_{os} = \sum_i G_i/K_{os}$,[9,23] which is a measure of the relative strength of the stress terms to the magnitude of $\Gamma(\mathbf{q})$ (eq 4). If the system is far from the spinodal point ($K_{os}$ is large) or is not well entangled ($G_N$ is small), this value is small, and hence the contribution of the stress terms to the magnitude of $\Gamma(\mathbf{q})$ is relatively small. Therefore, as $r$ is increased, enhancement of the concentration fluctuations becomes remarkable, due to the coupling effects. In this calculation, to reproduce the experimental scattering patterns around $W_i = 1^{1-3}$ as properly as possible, $r = 0.93$, and hence $r_0 \equiv \partial^2 f/\partial\phi^2 = K_{os}/\phi^2 = \sum_i G_i/r\phi^2 = 5.5 \times 10^4$ Pa was used.[23] $L$ was also chosen so that the experimental results were appropriately reproduced. The value $r_0$ corresponds to the value for solution A. This point will be discussed later. $\xi$ was assumed to be 10 nm,[30] from which $C$ was estimated by using $\xi \equiv (C/r_0)^{1/2}$.

**3.2. Structure Factor.** In this section, we present the calculated results on the two-dimensional and one-dimensional structure factors for solution A. The parameters used are summarized in Table 3. The structure factor $S(\mathbf{q};W_i)$ is obtained by normalizing $I(\mathbf{q};W_i)$ with respect to that in the quiescent state at $q = 0$:

$$S(\mathbf{q};W_i) \equiv I(\mathbf{q};W_i)/I(\mathbf{q}{=}0;W_i{=}0) \qquad (15)$$

Figure 3 shows the contour plots of $S(\mathbf{q})$ in the $q_x-q_y$ plane (i.e., $S(q_x,q_y,q_z{=}0) \equiv S(q_x,q_y)$) for a sequence of $W_i = 0.5$, 1.0, 5.0, and 10. In the quiescent state ($W_i = 0$), $S(q_x,q_y)$ is isotropic, and the intensity is almost equal to 1 over the $q$ range covered in Figure 3 ($0 < q < 5.0 \times 10^{-5}$ nm$^{-1}$). This indicates that at $W_i = 0$ the stress terms in $\Gamma(\mathbf{q})$ (eq 4) and the effect of convection (eq 6) vanish, and $S(\mathbf{q})$ reduces to the Ornstein−Zerinicke function in the absence of shear flow, i.e., $S(\mathbf{q}) = 1/(1 + q^2\xi^2)$. At $W_i = 0.5$, the intensity is slightly enhanced in the first and third quadrants, while suppressed in the second and the fourth quadrants, creating two sets of symmetric lobes with respect to the origin. These trends are caused mainly by the effect of shear stress as discussed before. At $W_i = 1.0$, the maxima in the first and third quadrants and the minima in the second and the fourth quadrants are clearly discerned. The origin of this peak will be discussed later. The shapes of the lobes are distorted around the origin, which is a result of the convection as verified by Milner[9] by artificially turning off the convective effects. At

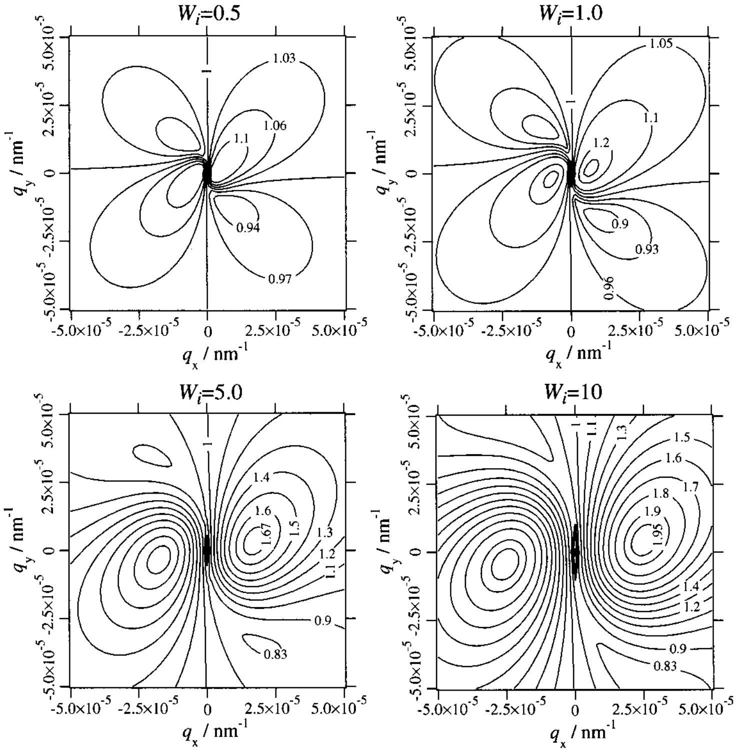

**Figure 3.** Contour plots of $S(q_x,q_y) \equiv S(q_x,q_y,q_z{=}0)$ calculated for a parameter set (Tables 2 and 3) suitable for solution A and for a sequence of $W_i = 0.5$, 1.0, 5.0, and 10. The intensity is normalized with respect to that at $W_i = 0$ and at $q = 0$. All the patterns have a 2-fold symmetry on rotation around $q_z$.

$W_i = 5.0$, the intensity enhancement is further progressed and the distortion becomes more pronounced. This pattern qualitatively agrees with the LS pattern measured by Wu et al.[1] At $W_i = 10$, the positions of the maxima move toward the higher $q$-region and align along a line nearly parallel to the horizontal axis. The rotation of the maxima with increasing $W_i$ also agrees with the observation of Wu et al.,[1] but the shift toward the higher $q$ region does not. The effect of $N_1$ on $S(q_x,q_y)$ will be discussed in section 4.3.

Figure 4 shows the contour plots of $S(\mathbf{q})$ in the $q_x$−$q_z$ plane (i.e., $S(q_x,q_y{=}0,q_z) \equiv S(q_x,q_z)$) for a sequence of $W_i = 0.1$, 0.5, 1.0, and 10. The $q$ range covered is the same as that in Figure 3. In the quiescent state, $S(q_x,q_z)$ is also isotropic, and the intensity is almost equal to 1 over the $q$ range covered in Figure 4. At $W_i = 0.5$, the intensity is slightly enhanced along $q_x$, showing a pair of symmetric wings with respect to $q_z$ axis. This is called the "butterfly" pattern that has been observed by LS and SANS experiments.[2−5,7] With increasing $W_i$, the intensity of the wings of the butterfly increases and the peak position moves toward the higher $q$ region, which is in accordance with the behavior in the $q_x$−$q_y$ plane. In addition, the wings of the butterfly spread in the $q_x$−$q_z$ plane so that the angle between two nearly straight contour lines with $S(q_x,q_z) = 1$ becomes small; hence, the dark streak is gradually narrowed. These results qualitatively agree with our results, except the shift of the peak position. Along $q_z$ direction, the intensity is suppressed in the low $q$ region, creating the contour lines with intensity smaller than 1 elongated along $q_z$ (see the cases of $W_i = 1$, 10). This trend will be discussed later.

Figure 5a shows the one-dimensional intensity profiles along the flow direction $S(q_x) \equiv S(q_x,q_y{=}0,q_z{=}0)$ from $W_i = 0$ up to 10. Figure 5b is the corresponding profiles when $N_1 = 0$, which is to be discussed later. In the absence of shear, $S(q_x)$ is identical with the Ornstein−Zernicke (OZ) function $S(q_x) = 1/(1 + \xi^2 q_x^2)$. The $q$ region covered in Figure 5 is satisfying $q_x\xi < 1$, thus $S(q_x) \cong 1$. At higher $q_x$ edge, the intensity starts to decrease toward the power law region ($S(q_x) \sim q_x^{-2}$) since this $q$ region is close to $\xi^{-1} = 0.1$ nm$^{-1}$. With increasing $W_i$, the peak position $q_{mx}$ shifts toward the higher $q$ region, and the peak intensity increases. In addition, the sharpness of the peak becomes more pronounced with $W_i$. It should be noted that the intensity for $W_i = 5.0$ and 10 in the low $q_x$ region is suppressed compared to the quiescent state while that for $W_i = 0.5$ is enhanced. This trend will be discussed later.

Figure 6a shows the one-dimensional intensity profiles along the neutral direction $S(q_z) \equiv S(q_x{=}q_y{=}0,q_z)$ from $W_i = 0$ up to 10. Figure 6b is also the corresponding profiles when $N_1 = 0$. In the $q_z$ region higher than about $10^{-4}$ nm$^{-1}$, the intensities for all $W_i$ are identical with that at $W_i = 0$ as will be discussed later. In the $q_z$ region lower than about $10^{-4}$ nm$^{-1}$, the intensity drops down to a certain level. The intensity level in this $q_z$ region becomes lower with increasing $W_i$ as will be discussed later in section 4.3.

## 4. Discussion

### 4.1. Applicability of This Theory.

The present study is the first attempt to calculate the structure factor in the $q_x$−$q_z$ plane at $W_i > 1$. Before discussing various features of the calculated results, we shall consider to what kind of systems this calculation can apply. The linearization with respect to concentration and the use of the Kaye−BKZ constitutive equation allow the viscoelasticity to behave nonlinearly but the concentration fluctuations to behave linearly. An ex-

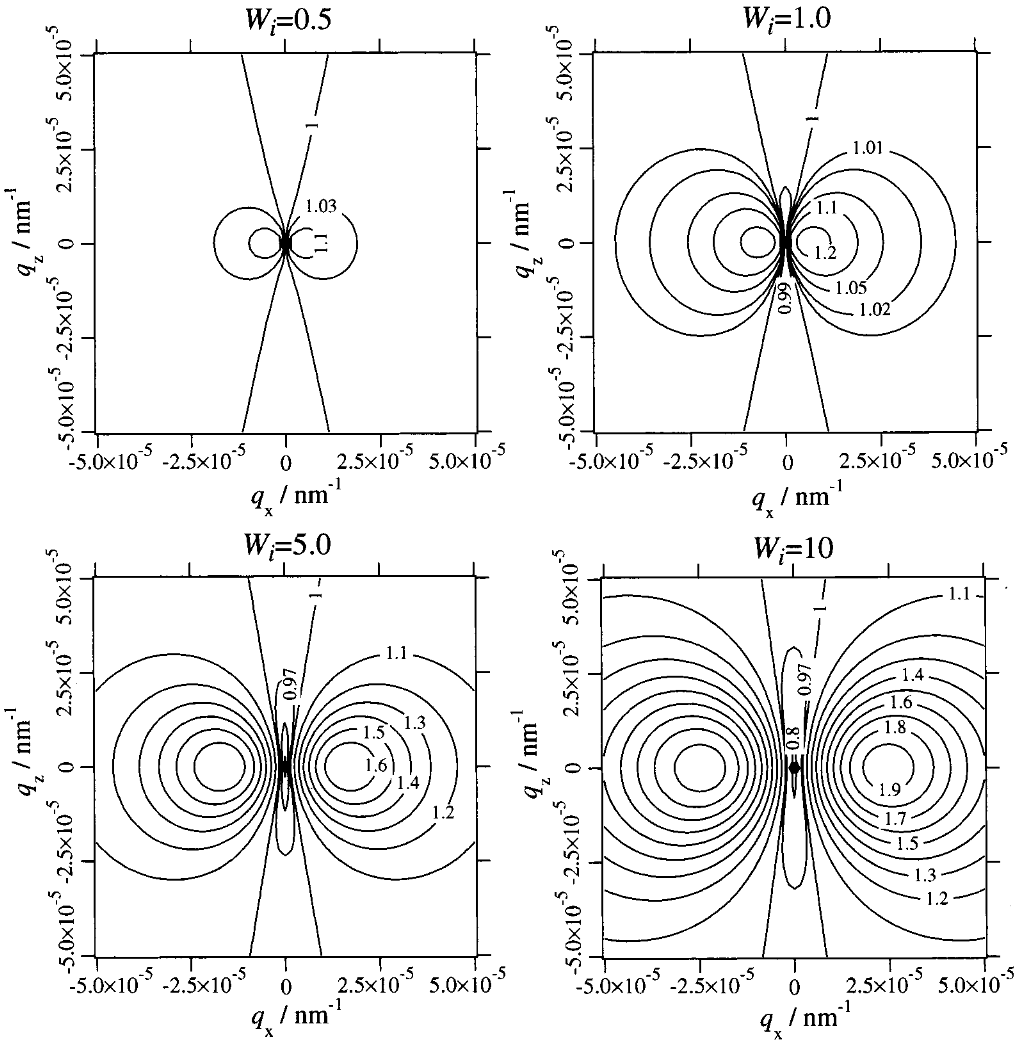

**Figure 4.** Contour plots of $S(q_x,q_z) \equiv S(q_x,q_y{=}0,q_z)$ calculated for the same set of the parameters as in Figure 3 and for a sequence of $W_i = 0.5$, 1.0, 5.0, and 10. The intensity is normalized with respect to that at $W_i = 0$ and at $q = 0$. All the patterns have the same rotational symmetry as described in Figure 3.

ample of such a situation is a system far away from the phase boundary where the system is relatively stable thermodynamically. In this case, the amplitude of the concentration fluctuations is expected to be small even at a high $\dot{\gamma}$; hence, the linear approximation could describe the enhanced concentration fluctuations by shear flow even under nonlinear viscoelastic response.

**4.2. $q_m$ and $I_m$ as a Function of $W_i$.** Let us first consider why the scattering peaks in Figures 3−5 are observed. For this purpose, the plot of $\Gamma(\mathbf{q})/q^2$ against $q^2$ is effective. To underline the feature of the $\Gamma(\mathbf{q})/q^2$ vs $q^2$ plot and also to avoid complexity, we shall concentrate on a special, simple case where it is assumed that $N_1 = 0$ and $q_x = q_y = q$ (a line in the $q_x$−$q_y$ plane with the angle of 45° with respect to $q_x$ axis). First, we shall look at the details of $\Gamma(\mathbf{q})/q^2$ vs $q^2$ plot in the absence of the convective effect. In this case, $\Gamma(\mathbf{q})$ in eq 4 is reduced to $\Gamma(\mathbf{q}) = L[q^2(r_0 + Cq^2) - (2q^2/\phi)(\partial\sigma_{xy}/\partial\phi)]$, and hence $\Gamma(q)/q^2 = L[(r_0 + Cq^2) - (2/\phi)(\partial\sigma_{xy}/\partial\phi)]$. As illustrated in Figure 7a, we focus on the thermodynamic term, $L(r_0 + Cq^2)$, and the stress term, $-(2L/\phi)(\partial\sigma_{xy}/\partial\phi)$, separately. In a single phase state ($r_0 > 0$), $L(r_0 + Cq^2)$ linearly increases with an increase of $q^2$ with an intercept of $Lr_0$ at $q^2 = 0$ and a slope of $LC$. On the other hand, $-(2L/\phi)(\partial\sigma_{xy}/\partial\phi)$ takes a negative constant value against $q^2$. $\Gamma(q)/q^2$ is given by the sum of these two terms. If $r_0 > (2/\phi)(\partial\sigma_{xy}/\partial\phi)$ (case (i) in Figure 7), $\Gamma(\mathbf{q})/q^2$ is always positive, and hence $\Gamma(q)$ never has a minimum at $q \neq 0$. If $r_0 < (2/\phi)(\partial\sigma_{xy}/\partial\phi)$ (case (ii) in Figure 7), on the contrary, there is a $q$ value satisfying $\Gamma(q)/q^2 = 0$, and $\Gamma(q)$ has a minimum at $q$ ($\neq 0$), as shown in Figure 7b. Thus, $S(q)$ has a maximum. This argument is equivalent to that of the early stage of the spinodal decomposition in a binary mixture in the absence of shear flow.

However, when we take the convective effect into account, the situation becomes complicated. The convective effect brings a fluctuation of a given $q$-Fourier mode toward a large $q$-Fourier mode. $\Gamma(q)$ with the convective effect on the above assumption is of the form $\Gamma(q) = L[Pq^2(r_0 + CPq^2) - (2Qq^2/\phi)(\partial\sigma_{xy}/\partial\phi)]$ with $P = \dot{\gamma}^2t^2 + 2\dot{\gamma}t + 2$ and $Q = 1 + \dot{\gamma}t$; hence, $\Gamma(q)/q^2 = L[P(r_0 + CPq^2) - (2Q/\phi)(\partial\sigma_{xy}/\partial\phi)$. Since $P$ increases more rapidly with time than $Q$, the contribution of the thermodynamic term becomes increasingly dominant with time. This indicates that even the fluctuations with $\Gamma(q) < 0$, which occurs when $r_0 < (2/\phi)(\partial\sigma_{xy}/\partial\phi)$ according to the above argument, cannot grow indefinitely, and these fluctuations would relax ultimately, provided the magnitude of the stress term is relatively small. In the case that the magnitude of the stress term is relatively large, the enhanced fluctuations grow indefinitely, and the scattering intensity diverges ultimately as discussed later.

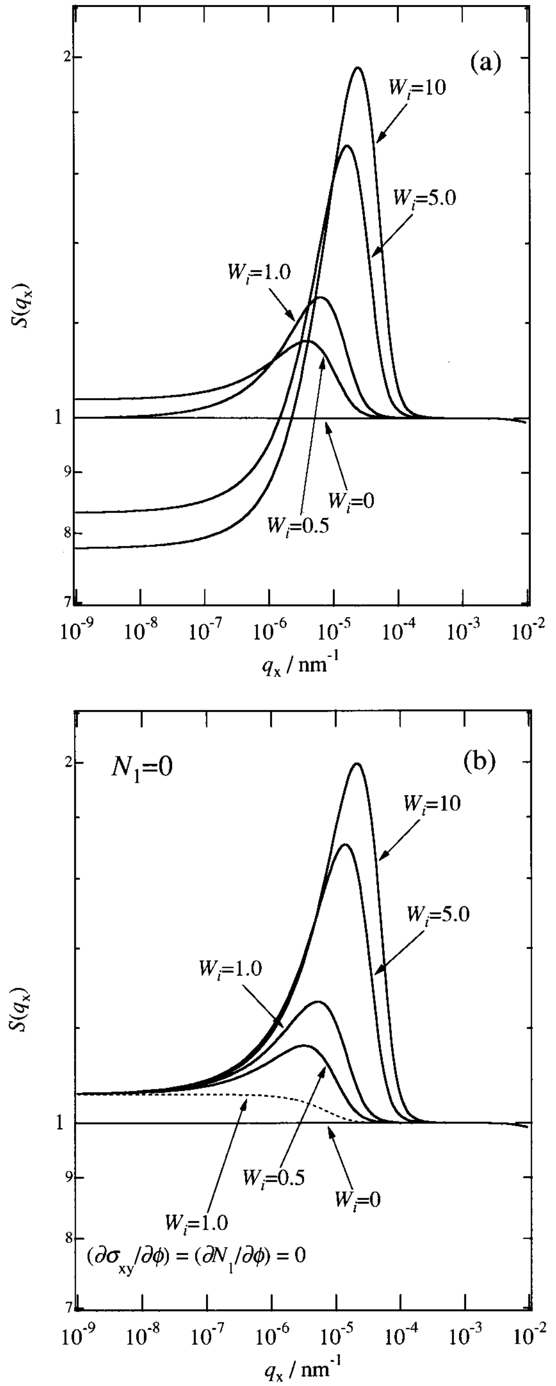

**Figure 5.** Theoretical intensity profiles along the flow direction $S(q_x) \equiv S(q_x,q_y=q_z=0)$ for the same set of the parameters as in Figure 3. (a) $N_1 \neq 0$. (b) $N_1 = 0$. The dotted line in (b) indicates the profile obtained with $\sigma_{xy} = N_1 = 0$ and with $W_i = 1.0$.

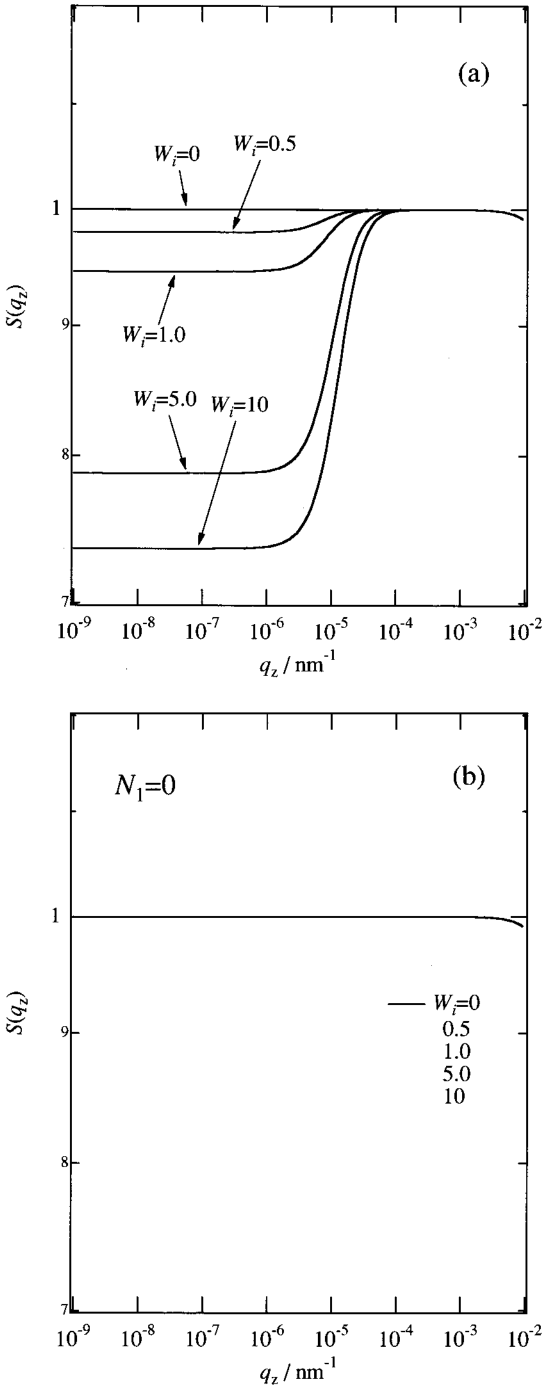

**Figure 6.** Theoretical intensity profiles along the neutral direction $S(q_z) \equiv S(q_x=q_y=0,q_z)$ for the same set of the parameters as in Figure 3. (a) $N_1 \neq 0$; (b) $N_1 = 0$.

In the same way, we can explain why the peak position $q_{mx}$ in $S(q_x)$ moves toward higher $q$ region with increasing $W_i$. This is due to the increasing magnitude of the stress term in $\Gamma(q)$ with $W_i$: As $W_i$ increases, the magnitude of the stress term $(-(2L/\phi)(\partial\sigma_{xy}/\partial\phi))$ increases, and hence the value of $q$ satisfying $\Gamma(q)/q^2 = 0$ moves toward higher $q$. Thus, $q_m$ increases with increasing $W_i$. This corresponds to the case of the spinodal decomposition where the peak position appeared in the early stage moves toward higher $q$ by quenching a binary mixture more deeply into the unstable region.

Thus, we have discussed the meaning of the peak and its $W_i$ dependence, and this tendency of the peak shift with $W_i$ is the same as the previous numerical calculation[9,11] as pointed out before, although the constitutive equation for the stress term employed in this work is different from theirs.[31] Therefore, we might say that these trends are due to the linear approximation of the HFMO theory in terms of concentration fluctuations. However, these trends are inconsistent with the experimental results ever reported. Here we shall introduce two experiments by Wu et al. and by us, to compare the present calculation with experiments in terms of the shift of $q_m$ and $I_m$ with $W_i$, although the two experiments differ in the experimental geometry.

Wu et al. obtained the steady-state structure factor of a semidilute PS/DOP solution ($M_w$ of PS is $1.8 \times 10^6$

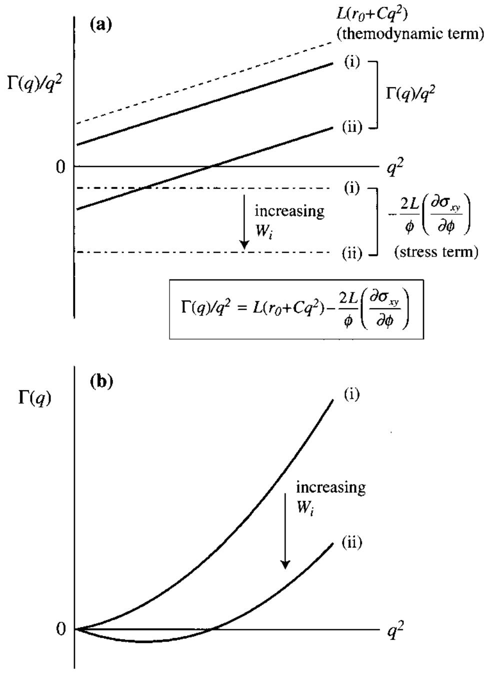

**Figure 7.** (a) Schematic illustration of $q^2$ dependence of $\Gamma(q)/q^2$. The broken line represents the thermodynamic term $L(r_0+Cq^2)$, and dash−dot line represents the stress term $-(2L/\phi)(\partial\sigma_{xy}/\partial\phi)$. $\Gamma(q)/q^2$ (bold line) is given by the sum of these two terms. In case (i) where $r_0 > (2/\phi)(\partial\sigma_{xy}/\partial\phi)$, $\Gamma(q)/q^2$ is always positive. In case (ii) where $r_0 < (2/\phi)(\partial\sigma_{xy}/\partial\phi)$, there is a $q$ value satisfying $\Gamma(q)/q^2 = 0$. This is brought by increasing $W_i$. (b) Schematic illustration of $q^2$ dependence of $\Gamma(q)$. In case (i), $\Gamma(q)/q^2$ is positive; hence, $\Gamma(q)$ monotonically increases with $W_i$. In case (ii), on the contrary, $\Gamma(q)/q^2$ is negative at low $q$ region, giving a minimum in $\Gamma(q)$. Hence, the peak emerges in the structure factor.

and a volume fraction of 0.04) under continuous shear flow in the $q_x - q_y$ plane.[1] At $W_i = 0.23$, the scattering maxima appeared in the first and third quadrants. As $W_i$ increased, the maxima rotated clockwise around the origin with *decreasing* $q_m$. This indicates that the characteristic size of the shear-induced fluctuations becomes large with increasing $W_i$ even at $W_i \lesssim 1$.

Let us introduce in detail another experimental data by us. We conducted LS measurement on semidilute PS/DOP solutions under continuous shear flow to investigate the steady state scattering intensity in the $q_x - q_z$ plane. Two PS/DOP solutions were employed. In one solution (solution B, see Table 1 for characteristics), the concentration is 4.0 wt %, which is 3.1 times as concentrated as the overlap concentration ($c/c^* = 3.1$). The measurement was carried out at 15.0 °C, which is 0.8 °C higher than the cloud point (14.2 °C). In another solution (solution C), the measurement was carried out at 9.0 °C. Although the cloud point of this solution has not been determined, the solution is clearly in a single phase at 9.0 °C. The details of the shear LS apparatus and the experimental methods have been reported elsewhere.[2,24]

Figure 8 shows the scattering profiles along $q_x$ and $q_z$ for solution C. Along $q_x$, a broad scattering peak appears at $W_i = 1.03$. With increasing $W_i$, $q_{mx}$ moves to the low $q_x$ region and $I_m$ increases. This implies that the characteristic size of the shear-induced structure becomes large. Beyond $W_i \geq 16.3$, the peak cannot be discerned, because $q_{mx}$ goes outside our experimental $q$ window. On the other hand, along $q_z$, there is clearly a maximum at $W_i = 6.50$. However as $W_i$ increases in the range of $W_i > 6.50$, the scattering maximum disappears and then intensity also increases over the $q$ region covered in this experiment. These experimental results will be reported elsewhere.[25]

The difference in the peak shift with $W_i$ between the present numerical calculation and the experiment might be realized more systematically by comparing the results in Figures 9 and 10; the changes in $q_{mx}$ and $I_{mx}$ with $W_i$ estimated from Figure 5a (numerical calculation) and estimated from Figure 8 (experiments) are plotted respectively in Figures 9 and 10. The dotted lines in Figure 9 are those obtained with $N_1 = 0$, which is to be discussed later. In Figure 10, the filled triangles denote the data for solution B and the open circles denote those for solution C. Figure 9 shows that both $q_{mx}$ and $I_{mx}$ monotonically increases with $W_i$ on the double-logarithmic scale.

On the other hand, in Figure 10, the trend in $q_{mx}$ with $W_i$ is quite opposite to that of Figure 9. At $W_i < 4$, $q_{mx}$ decreases with $W_i$ with exponents of −0.35 for solution B and −0.90 for solution C, respectively, indicating that the characteristic size of the shear-induced structure becomes large.

Note that there is a large difference between the value of $r$ (defined in sec. 3.1.2) for solutions B and C and the present numerical analysis effective for solution A, while the viscoelastic properties in these systems are not so different. The value $r$ for solution B at 15.0 °C is estimated to be $3.9 \times 10^{-2}$, which is much lower than $r = 0.93$ employed in this calculation.[26] This means that the numerical analysis was carried out at the temperature very close to the spinodal point since $r$ becomes smaller as temperature is decreased toward the spinodal point as described before. This point, the difference in $r$, will be discussed in section 4.4.

However, we think that the discrepancy between the two in terms of the shift of $q_{mx}$ with $W_i$ may be primarily caused by the neglect of the higher-order terms in free energy functional in the linearized theory rather than the difference in the value $r$, since the higher-order terms cause the coarsening of the structures. The details of the coarsening or the evolution of the shear-induced structure with increasing $W_i$ has been experimentally revealed in the $q_x - q_z$ plane with LS.[3] At a given temperature, the $W_i$ dependence of LS intensity from the solution was found to be classified into four regimes: regime I at $W_i < W_{i,cx}$, where $W_{i,cx}$ is the critical Wisenberg number for the shear-induced enhancement of concentration fluctuations and/or phase separation, and regime II−IV at $W_i > W_{i,cx}$. In regime I, no change is observed in LS; hence, the concentration fluctuations as observed in the $q_x - q_z$ plane is essentially identical to those in the quiescent state. In regime II, a butterfly pattern appears with a dark streak along $q_z$. As $W_i$ increases, the butterfly develops in such a way that the scattering intensity increases along $q_x$, the wing expands, and the dark streak narrows. In this regime, $I(q_z)$ starts to increase from $I(q_z)$ at rest above a certain $W_i$ (designated hereafter $W_{i,cz}$). The details in regime III and IV have been elucidated in our previous works.[3] For solutions B and C, there is a relationship $W_{i,cx} \lesssim W_i = 1 < W_{i,xz}$.

In regime II, $W_{i,cz}$ is believed to be the critical shear rate at which the shear-induced plane wave fluctuations turn into the phase-separated structures,[5,7] a basis of which is that the phase-separated structures convected

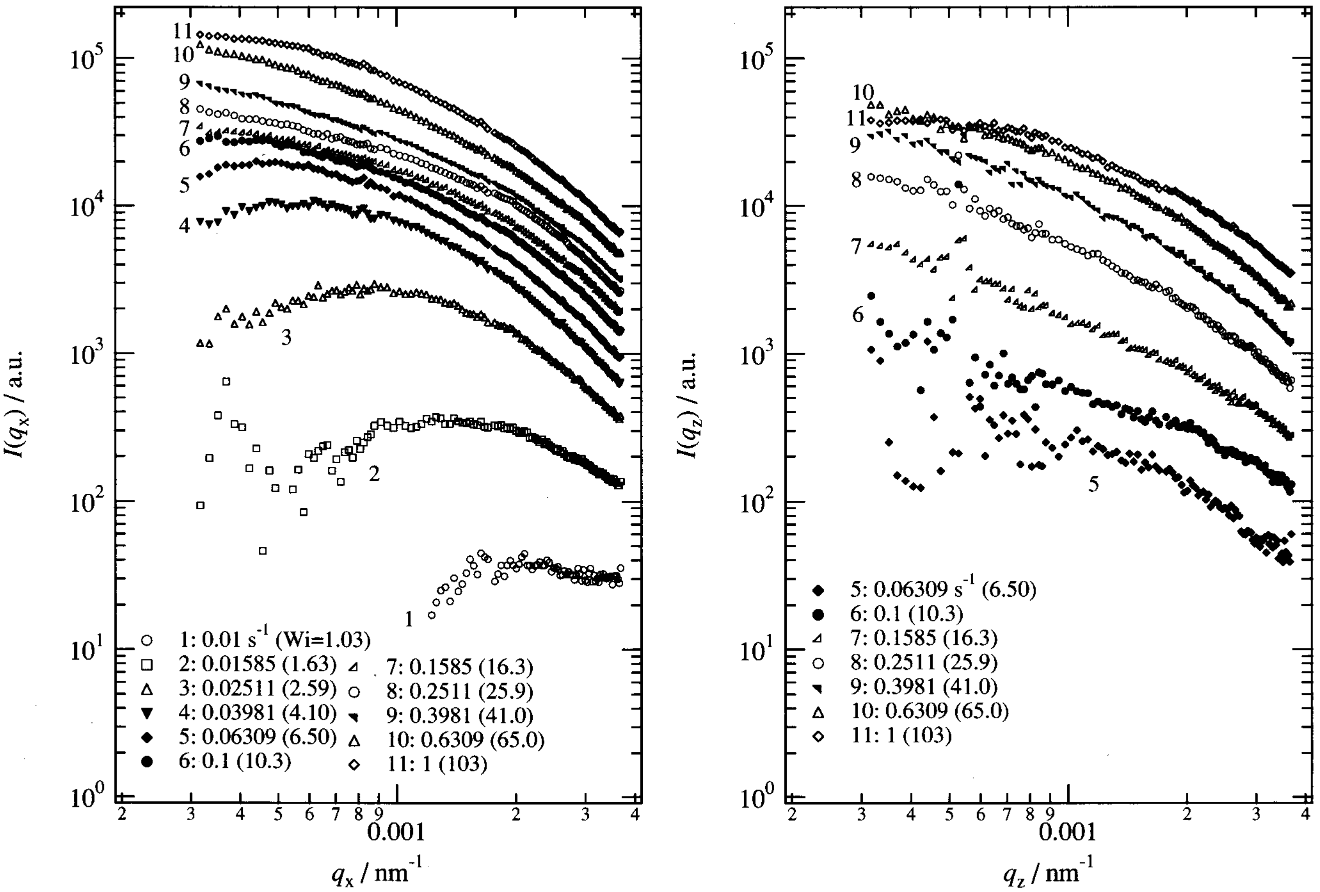

**Figure 8.** Scattering intensity profiles along the flow (a) and the neutral (b) direction for solution C for a series of shear rates (or Weisenberg number $W_i$).

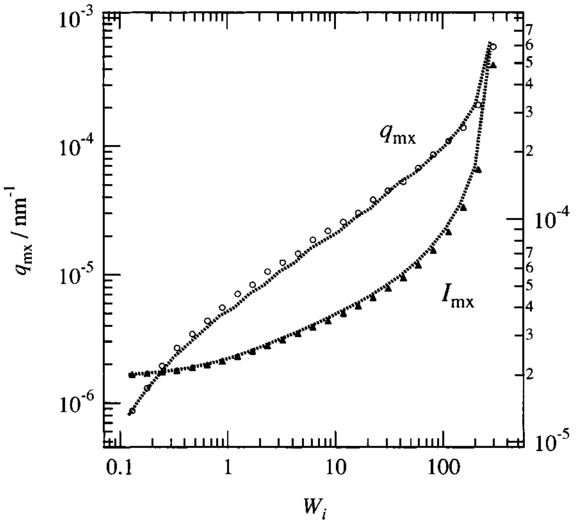

**Figure 9.** Theoretical results on $q_{mx}$ (open circles) and $I_{mx}$ (filled triangles) as a function of $W_i$ for the same set of the parameters as in Figure 3 for the case of $N_1 \neq 0$. The dotted lines are those obtained for the case of $N_1 = 0$.

by shear flow bring about the excess scattering along $q_z$. This means that below $W_{i,cz}$ the structures induced are essentially no more than the enhanced concentration fluctuations, not the phase-separated structures, and hence the linear theory could be applicable, provided the amplitude of the fluctuations is small.

However, even at $W_i \sim 1$, the value of which is almost identical with $W_{i,cx}$ and even smaller than $W_{i,cz}$, the enhanced concentration fluctuations cannot be predicted by the linear theory; i.e., the shifts of $q_{mx}$ with $W_i$ disagree. The reasons might result from the following

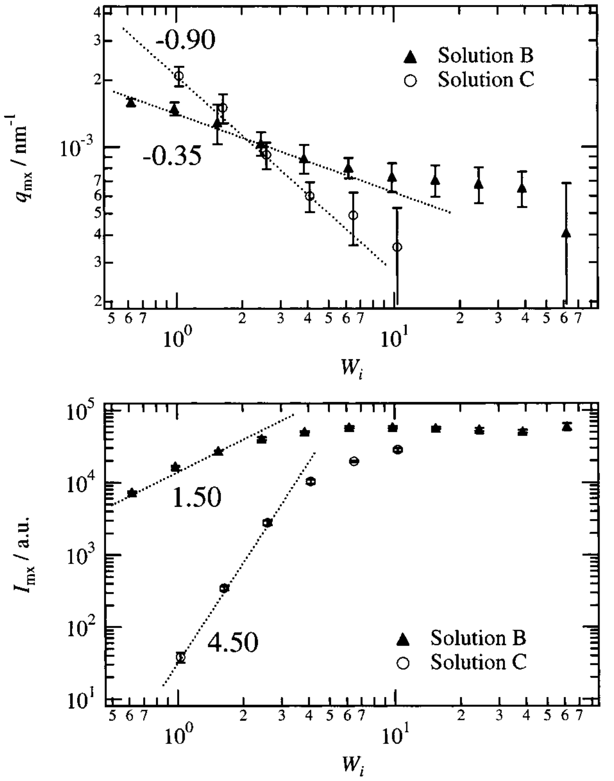

**Figure 10.** $q_{mx}$ (top) and $I_{mx}$ (bottom) as a function of $W_i$ for solutions B and C.

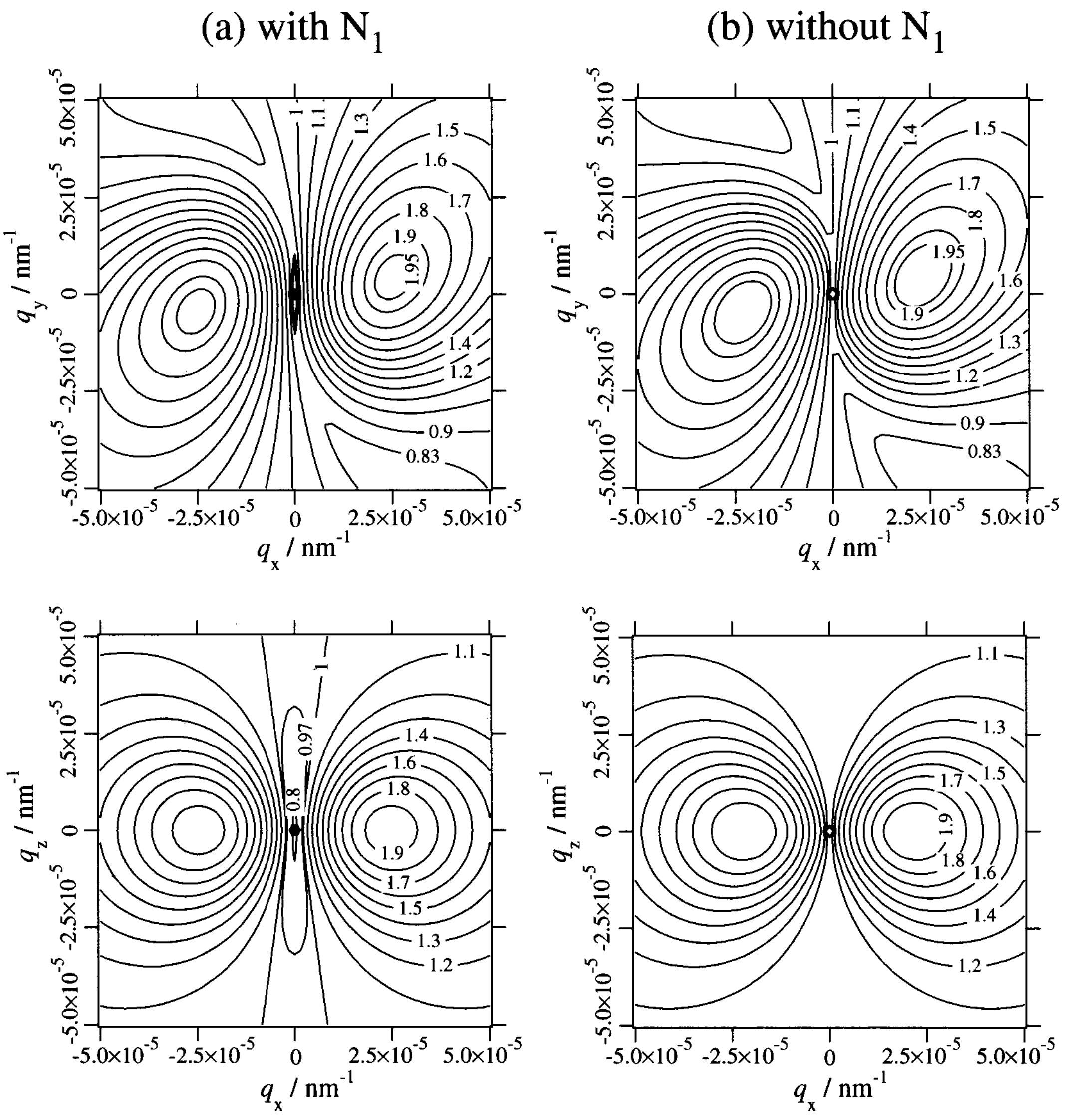

**Figure 11.** Comparison of $S(q_x,q_y)$ (upper row) and $S(q_x,q_z)$ (lower row) calculated for the same set of the parameters as in Figure 3 at $W_i = 10$ with $N_1 \neq 0$ (left, part a) and $N_1 = 0$ (right, part b).

two possibilities. First, under the situation where the shear-enhanced scattering is observed in the $q_x$–$q_z$ plane, the amplitude of the shear-induced fluctuations occurring in the actual system is too large to be predictable with the linear theory even at $W_i \sim 1$. This suggests that the enhanced concentration fluctuations that can be described by the linear theory is difficult to be detected in the $q_x$–$q_z$ plane experimentally. Second, the higher-order terms in the free energy functional in eq 1 cannot be negligible even at $W_i \sim 1$ where the amplitudes of the fluctuations are expected to be small enough. This means that the nonlinear effect plays an important role even for the enhanced concentration fluctuations with small amplitude.

To elucidate the above problems, the computer simulation based on the HFMO theory would be a strong tool. In fact, the simulation studies by Onuki et al.[16] and by Okuzono[19] which included the nonlinear terms in the free energy functional have shown the shift of $q_m$ toward the low $q$ region with increasing $W_i$, indicating that the coarsening effect is well reproduced. From a viewpoint of the quantitative comparison between the theory and the experiment, more detailed and quantitative theoretical analysis of the structure factor would be required by means of the three-dimensional computer simulation studies of the nonlinear dynamical equation of HFMO (eq 1) with a proper incorporation of the stress.

Finally, we have to note a striking difference in the $q$ region where the butterfly appears. It is illuminated, by comparing $q_{mx}$ predicted by the linear theory (Figure 5) and that observed in the experiments (Figure 8), that the butterfly of the numerical calculation appears in the $q$ region very much lower than that in the experiment by about 2 orders of magnitude. This $q$ region is obviously parameter dependent. We estimated a change in the value $q_{mx}$ at $W_i = 1$ upon changing the parameter $r$ from 0.1 to 4, keeping the rheological parameters ($\tau_i$, $G_i$, α, $\beta$) constant. We found $q_{mx}$ changes from $6.83 \times 10^{-7}$ to $2.79 \times 10^{-5}$ nm$^{-1}$. At $r > 4$, $I_{mx}$ diverged. On the other hand, experimentally, the $q$ region where the butterfly starts to emerge at low $W_i$ has been found to be around $10^{-3}$ nm$^{-1}$ as shown in Figure 8 or 10. This means that the difference in the $q$ region cannot be attributed to the choice of the parameters. This discrepancy in the $q$ region might reflect again the limitation of the linear theory employed in this work.

### 4.3. Effect of Normal Stress.

Upon substituting $N_1 = 0$ in eq 4 and analyzing the results obtained, we can examine the effect of $N_1$ on $S(\mathbf{q})$. Figure 11 shows the differences in $S(q_x,q_y)$ and $S(q_x,q_z)$ at $W_i = 10$ with and without $N_1$. The intensity distribution in the vicinity of the peaks is not affected much. Around $q_x = 0$, on the contrary, the intensities are lower than 1 when $N_1 \neq 0$ for both $S(q_x,q_y)$ and $S(q_x,q_z)$, creating contour patterns elongated along $q_y$ and $q_z$, respectively, and hence promoting the dark streak especially for $S(q_x,q_z)$. The suppression of the intensities along $q_y$ and $q_z$ is due to the normal stress, as has been already discussed in section 2.1.

The difference in the structure factor with and without $N_1$ is more quantitatively clarified in Figures 5b and 6b, where $S(q_x)$ and $S(q_z)$ are plotted as functions of $q_x$ and $q_z$, respectively, with and without $N_1$. In Figure 5b, when $N_1 = 0$, we cannot see any suppression of the intensity over the $q$ region covered, and the intensity is rather enhanced compared with the quiescent state due to the convective effect.[32] When $N_1 \neq 0$, on the other hand, the intensity is suppressed in the $q$ region lower than $q_{\mathrm{m}x}$ compared with those in Figure 5b. In addition, the suppression of the intensity is more significant with increasing $W_i$.

The same trend is found in Figure 6b. When $N_1 \neq 0$, the higher the value of $W_i$, the more the intensity is suppressed in the low $q$ region. When $N_1 = 0$, the profiles at all $W_i$ are all identical with that at $W_i = 0$. In other word, $\sigma_{xy}$ does not affect the concentration fluctuations along $q_z$. The reason that the intensity in the lower $q$ region is more suppressed than that in the higher $q$ region may be as follows: From eqs 4 and 6, we obtain $\Gamma(q_z) = Lq_z^2[(r_0 + Cq_z^2) + {}^1/_{(3\phi)}(\partial N_1/\partial\phi)]$. Thus, the normal stress suppresses the fluctuations. However, at a large $q_z$ mode, the contribution of the stress term to the maginitude of $\Gamma(\mathbf{q})$ is relatively small, and that of $Cq_z^4$ in the thermodynamic term is relatively large. Thus, the suppression of the intensity by $N_1$ is effective at small $q_z$'s but disappears at large $q_z$'s.

Next, we pay attention to $q_{\mathrm{m}x}$ and $I_{\mathrm{m}x}$. The dotted lines in Figure 9 are those estimated from $S(q_x)$ with $N_1 = 0$. The existence of $N_1$ slightly shifts $q_{\mathrm{m}x}$ to higher $q_x$ and slightly decreases $I_{\mathrm{m}x}$, due to the suppresion of the low $\mathbf{q}$ modes by $N_1$ as seen in Figure 5a. However, this changes in $q_{\mathrm{m}x}$ and $I_{\mathrm{m}x}$ are not so important compared with the remarkable suppression of the intensity in the low $q$ region. These trends may be due to that $q_{\mathrm{m}x}$ is located in the relatively large $q$ region, and the peak may avoid the suppression by $N_1$.

Now, we focus on the effect of $N_2$, which is assumed to be 0 in this calculation by the prediction of the separable Kaye−BKZ equation employed in this work. However, in the actual system, $N_2$ has a value of about $(-1/8)N_1$.[20] Taking account of the effect of $N_2$ on the relaxation rate (eq 4), we can obtain the modified relaxation rate by adding $({}^1/_3)(q_x^2 + q_y^2 - 2q_z^2)(\partial N_2/\partial\phi)$ inside the brackets of eq 4 without knowing the actual form of $N_2$ as a function of time and shear rate. In the same way as $N_1$, the coefficient of $N_2$ with the convective effect is $({}^1/_3)[(1 + \dot{\gamma}^2t^2)q_x^2 + q_y^2 - 2q_z^2 + 2\dot{\gamma}tq_xq_y]$. This means that the intensity would always tend to be suppressed along $q_x$ and $q_y$ and enhanced along $q_z$, since $N_2 < 0$. In the $q_x$−$q_y$ plane, this coefficient ($q_z = 0$) is always positive; hence, $N_2$ works to suppress the fluctuations in this $q$ region. It should be noted that the effect of $N_2$ cannot be neglected at high $W_i$, which is one of the difficulties in our calculation.

**4.4. Shear-Induced Instability.** As shown in Figures 3−5, the intensity around $\mathbf{q}_{\mathrm{m}}$ increases with increasing $W_i$. Further investigations of the $W_i$ dependence of the intensity distribution revealed that the intensity diverges around $\mathbf{q}_{\mathrm{m}}$ at $W_i$'s greater than a certain high $W_i$.

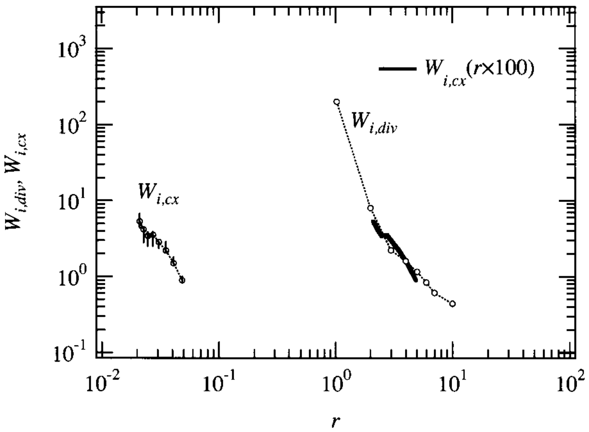

**Figure 12.** $r$ dependence of theoretical $W_{i,\mathrm{div}}$ calculated for the same set of the parameters as in Figure 3 and experimental $W_{i,cx}$ (for solution A). $W_{i,\mathrm{div}}$ is defined as the Weisenberg number at which the intensity along $q_x$ diverges at nonzero value of $q_{\mathrm{m}x}$. The bold line on the line of $W_{i,\mathrm{div}}$ indicates $W_{i,cx}$ shifted horizontally ($r \times 100$).

This also means that the shear flow brings about instability in the solution at a particular $q$ mode with a finite wavenumber $q_{\mathrm{m}}$ ("mesoscopic instability"). In other words, the shear flow quenches the solution inside the *apparent* spinodal line. Here we define $W_{i,\mathrm{div}}$ as $W_i$ at which the intensity $S(q_x)$ diverges. We examined $W_{i,\mathrm{div}}$ as a function of $r$ and plot it in Figure 12. As already explained, $r$ is a measure of the relative strength of the stress terms against thermodynamic terms on the shear-induced concentration fluctuations in eq 4. If the solution is far from the spinodal temperature ($K_{\mathrm{os}}$ is large) or is not well entangled ($G_{\mathrm{N}}$ is small), the value of $r$ is small. Figure 12 indicates that $W_{i,\mathrm{div}}$ increases with decreasing $r$.

Now we try to consider this result in conjunction with the experiments. Until now, there is no experimental study reporting the shear-induced instability. However, we have found a critical shear rate $W_{i,cx}$ at which the butterfly pattern starts to emerge in the $q_x$−$q_z$ plane.[3] $W_{i,cx}$, measured as a function of the temperature at various concentrations with varying the solvent quality, is a measure of the relative ease of bringing the shear-induced concentration fluctuations reflected in the $q_x$−$q_z$ plane as a function of these parameters, and we may regard $W_{i,cx}$ as the value having the meaning parallel to $W_{i,\mathrm{div}}$. Experimentally, we have already obtained the temperature dependence of $W_{i,cx}$ at various concentration and estimated $W_{i,\mathrm{cx}}$ as a function of $r$, the details of which has been reported elsewhere.[28]

In Figure 12, $W_{i,\mathrm{cx}}$ obtained for solution A is also plotted as a function of $r$.[28] $W_{i,cx}$ was obtained by changing the temperature from 15.7 °C ($T - T_{\mathrm{cl}} = 1.9$ °C) to 50° ($T - T_{\mathrm{cl}} = 36.2$ °C). A comparison between $W_{i,\mathrm{div}}$ and $W_{i,cx}$ reveals two important features. One is that $W_{i,cx}$ is observed in a range of $r$ about 2 orders of magnitude lower than that of $W_{i,\mathrm{div}}$. To consider what it means, we shall assume that $W_{i,cx}$ and $W_{i,\mathrm{div}}$ are almost identical, rather than parallel. On this assumption, this feature indicates that the determination of $W_{i,\mathrm{div}}$ by the present calculation requires quite large values of $r$ compared with those encountered in a real system. This also means that the value of $r$ (=0.93) for the calculation for the structure factors presented in

Figures 3−6 is also much larger than that of the real system. When $r$ was chosen consistently with the real system, the magnitude of the stress terms in $\Gamma(\mathbf{q})$ were too small, and the enhancement of the intensity of the structure factor was too small even at around $W_i = 1$ where the butterfly pattern starts to appear in the real system. These trends may imply that the effects that the present calculation neglected, such as the higher-order terms in the free energy functional and the mode−mode coupling associated with the higher-order terms that would promote the coarsening of the structures, are really important in the real system.

The other feature is that there is a parallel relation between $W_{i,cx}$ and $W_{i,\mathrm{div}}$ as a function of $r$ as we have assumed above. The bold line in Figure 12 indicates $W_{i,\mathrm{cx}}(r\times 100)$, and we find that $W_{i,\mathrm{div}}(r)$ and $W_{i,\mathrm{cx}}(r\times 100)$ are almost in agreement. This parallel relation would be useful to predict the enhancement of the concentration fluctuations observed in the $q_x-q_z$ plane.

## 5. Summary

Most of SALS and SANS experimental studies concerning shear-enhanced concentration fluctuations in the semidilute polymer solutions under continuous shear flow were conducted in the $q_x-q_z$ plane. Moreover, the shear-enhanced SALS and SANS were observed in most of the cases in non-Newtonian regime at $W_i \gtrsim 1$ where the shear thinning is remarkable. To analyze the experimental results obtained under these situations, we conducted numerical analysis of the HFMO theory coupled with the Kaye−BKZ equation.

Using the theory described above, we have shown the structure factors, not only in the $q_x-q_y$ plane but also in the $q_x-q_z$ plane, within the linear approximation in terms of the concentration fluctuations. Incorporation of the distribution of relaxation time and modulus for $\sigma_{xy}$ and $N_1$ enables us to calculate the structure factor at $W_i \gtrsim 1$ in the $q_x-q_z$ plane, which have not been obtained in the previous studies, despite the desire to compare the existing theory with the experimental results in the $q_x-q_z$ plane at $W_i \gtrsim 1$. Although the resulting theoretical structure factor explained qualitatively important features of the experimental structure factors in its shape, we found serious discrepancies between them in the following points: the $q$ region where the excess scattering due to the shear-induced structures emerges is much lower than that found in the experiments, and the theoretical $q_{\mathrm{m}x}$ increases with increasing $W_i$, while the experimental $q_{\mathrm{m}x}$ decreases with $W_i$. This may indicate the limits of the linearization approximation adopted in this work and the importance of the higher order terms in the free energy functional that were neglected in the present calculation.

We have checked how $N_1$ affects the structure factor. The existence of $N_1$ suppresses the intensity at $q < q_{\mathrm{m}}$. This trend is more remarkable with increasing $W_i$, promoting the characteristic features of dark streak in the contour pattern in the $q_x-q_z$ plane.

The $r$ dependence of $W_{i,\mathrm{div}}$ has been also investigated, where $r$ is the ratio of the plateau modulus to the osmotic modulus and $W_{i,\mathrm{div}}$ is $W_i$ at which the calculated intensity diverges at nonzero value of $q_{\mathrm{m}}$, and hence the microphase instability is induced. A decrease of $r$ increases $W_{i,\mathrm{div}}$, corresponding to the experimental results such that $W_{i,\mathrm{cx}}$ increases with increasing temperature, implying the temperature dependence of the butterfly appearance is qualitatively parallel to the temperature dependence of $W_{i,\mathrm{div}}$.

**Acknowledgment.** We thank Professor Akira Onuki for valuable discussions throughout the course of the studies.

## Appendix

Here we shall derive the relaxation rate of the concentration fluctuations from eq 1. We first calculate $\nabla\cdot\nabla\cdot\boldsymbol{\sigma}^{(n)}$ on the right-hand side of eq 1. The mechanical stress tensor $\boldsymbol{\sigma}$ is generally written as

$$\boldsymbol{\sigma} = \begin{pmatrix} \sigma_{xx} & \sigma_{xy} & \sigma_{xz} \\ \sigma_{yx} & \sigma_{yy} & \sigma_{yz} \\ \sigma_{zx} & \sigma_{zy} & \sigma_{zz} \end{pmatrix} \tag{A1}$$

then we find

$$\nabla\cdot\nabla\cdot\boldsymbol{\sigma}^{(n)} = 2\frac{\partial^2}{\partial x\,\partial y}\sigma_{xy} + \frac{1}{3}\left[\frac{\partial^2}{\partial x^2}(2\sigma_{xx} - \sigma_{yy} - \sigma_{zz}) - \frac{\partial^2}{\partial y^2}(-\sigma_{xx} + 2\sigma_{yy} - \sigma_{zz}) - \frac{\partial^2}{\partial z^2}(-\sigma_{xx} - \sigma_{yy} + 2\sigma_{zz})\right] \tag{A2}$$

$$= 2\frac{\partial^2}{\partial x\,\partial y}\sigma_{xy} + \frac{1}{3}\left[\left(2\frac{\partial^2}{\partial x^2} - \frac{\partial^2}{\partial y^2} - \frac{\partial^2}{\partial z^2}\right)N_1 + \left(\frac{\partial^2}{\partial x^2} + \frac{\partial^2}{\partial y^2} - 2\frac{\partial^2}{\partial z^2}\right)N_2\right] \tag{A3}$$

Here we can put $N_2 = 0$, because a special case of a separable Kaye−BKZ equation[20] employed in this work predict it. Substituting eq A3 into linearized eq 1 yields a equation for $\delta\phi$ of the form

$$\left(\frac{\partial}{\partial t} + \mathbf{v}\cdot\nabla\right)\delta\phi = L\left\{\nabla^2(r_0 - C\nabla^2) - \frac{1}{\phi}\left[2\frac{\partial^2}{\partial x\,\partial y}\left(\frac{\partial\sigma_{xy}}{\partial\phi}\right) + \frac{1}{3}\left(2\frac{\partial^2}{\partial x^2} - \frac{\partial^2}{\partial y^2} - \frac{\partial^2}{\partial z^2}\right)\left(\frac{\partial N_1}{\partial\phi}\right)\right]\right\}\delta\phi \tag{A4}$$

where $L$ is the Onsager coefficient and

$$\frac{\delta F}{\delta\phi} = (r_0 - C\nabla^2)\delta\phi \tag{A5}$$

to linear order in $\delta\phi$ was used in eq 1. The coefficient $r_0$ is the second derivative of the Flory−Huggins free energy density for a semidilute solution with respect to $\phi$ given by

$$r_0 = \frac{k_{\mathrm{B}}T}{v_0}\left[\phi + (1 - 2\chi) + \frac{1}{N_w\phi}\right] \tag{A6}$$

where $k_{\mathrm{B}}$ is the Boltzmann constant, $T$ the absolute temperature, $v_0$ the volume of a monomer, $\chi$ the interaction parameter between polymer and solvent, and $N_w$ the weight-average polymerization index of the polymer used. The coefficient $C$ in eq A5 is related to the gradient free energy and is determined using the random-phase approximation as

$$C = \frac{k_{\mathrm{B}}T}{v_0}\frac{b^2}{36\phi} \tag{A7}$$

for polymer solution, where *b* is the statistical segmental length of polymer.

By the Fourier transformation of eq A4, we can obtain a equation for the Fourier component $\phi_{\mathbf{q}}$.

$$\left(\frac{\partial}{\partial t} - \dot{\gamma} q_x \frac{\partial}{\partial q_y}\right)\phi_{\mathbf{q}} = -L\left\{q^2(r_0 + Cq^2) - \frac{1}{\phi}\left[2q_xq_y\left(\frac{\partial \sigma_{xy}}{\partial \phi}\right) + \frac{1}{3}(2q_x^{\ 2} - q_y^{\ 2} - q_z^{\ 2})\left(\frac{\partial N_1}{\partial \phi}\right)\right]\right\}\phi_{\mathbf{q}} \quad \text{(A8)}$$

On the left-hand side of eq A8, use is made of $\mathbf{v}\cdot\nabla = \dot{\gamma}y(\partial/\partial x)$. Equation A8 indicates that the concentration fluctuations are convected by shear flow and relax with the following relaxation rate:

$$\Gamma(\mathbf{q}) = L\left\{q^2(r_0 + Cq^2) - \frac{1}{\phi}\left[2q_xq_y\left(\frac{\partial \sigma_{xy}}{\partial \phi}\right) + \frac{1}{3}(2q_x^{\ 2} - q_y^{\ 2} - q_z^{\ 2})\left(\frac{\partial N_1}{\partial \phi}\right)\right]\right\} \quad \text{(A9)}$$

## References and Notes

(1) Wu, X.-L.; Pine, D. J.; Dixon, P. K. *Phys. Rev. Lett.* **1991**, *66*, 2408.

(2) Hashimoto, T.; Fujioka, K. *J. Phys. Soc. Jpn.* **1991**, *60*, 356.

(3) Hashimoto, T.; Kume, T. *J. Phys. Soc. Jpn.* **1992**, *61*, 1839.

(4) Saito, S.; Koizumi, S.; Matsuzaka, K.; Suehiro, S.; Hashimoto, T. *Macromolecules* **2000**, *33*, 2153.

(5) Saito, S.; Hashimoto, T.; Morfin, I.; Lindner, P.; Boué, F. *Macromolecules*, in press.

(6) Boué, F.; Lindner, P. *Europhys. Lett.* **1994**, *25*, 421.

(7) Morfin, I.; Lindner, P.; Boué, F. *Macromolucules* **1999**, *32*, 7208.

(8) Helfand, E.; Fredrickson, G. H. *Phys. Rev. Lett.* **1989**, *62*, 2468.

(9) Milner, S. T. *Phys. Rev. E* **1993**, *48*, 3674.

(10) Onuki, A. *J. Phys.: Condens. Matter* **1997**, *9*, 6119.

(11) Ji, H.; Helfand, E. *Macromolecules* **1995**, *28*, 3869.

(12) Kaye, A. College of Aeronautics, Cranford, U.K., Note No. 134, 1962.

(13) Bernstein, B.; Kearsley, E. A.; Zapas, L. J. *Trans. Soc. Rheol.* **1963**, *7*, 391.

(14) Doi, M. In *Dynamics and Patterns in Complex Fluids*; Onuki, A., Kawasaki, K., Eds.; Springer: Berlin, 1990.

(15) Doi, M.; Onuki, A. *J. Phys. II* **1992**, *2*, 1631.

(16) Onuki, A.; Yamamoto, R.; Taniguchi, T. *J. Phys. II* **1997**, *7*, 295.

(17) Onuki, A.; Kawasaki, K. *Ann. Phys. (N.Y.)* **1979**, *121*, 456.

(18) Onuki, A.; Kawasaki, K. *Ann. Phys. (N.Y.)* **1981**, *131*, 217.

(19) Okuzono, T. *Mod. Phys. Lett. B* **1997**, *11*, 379.

(20) Larson, R. G. *Constitutive Equations for Polymer Melts and Solutions*; Butterworths: Boston, 1988.

(21) Laun, H. M. *Rheol. Acta* **1978**, *17*, 1.

(22) This assumption may be problematic, since the very short time response comes from the Rouse dynamics between entanglement points, the values of α and $\beta$ of which are different from an entangled solution. It may be a difficult problem, however, to distinguish the semidilute and dilute regions in a discrete relaxation spectra as will be presented in Table 2; hence, we shall use the values of α and $\beta$ for an entangled solution for $G_i$ and $\tau_i$ for all *i* for simplicity.

(23) $K_{\mathrm{os}}$ is defined as $K_{\mathrm{os}} \equiv \phi(\partial\pi/\partial\phi) = \phi^2(\partial^2 f/\partial\phi^2) = \phi^2 r_0$. The numerical value for $r_0$, $r_0 = 5.5 \times 10^4$ Pa, was obtained by using the value $\sum_i G_i$ estimated from Table 2, $r = 0.93$, and $\phi = 0.0568$ for solution A.

(24) Hashimoto, T.; Takebe, T.; Suehiro, S. *Polym. J.* **1986**, *18*, 123.

(25) Hattori, T.; Saito, S.; Hashimoto, T. Manuscript in preparation.

(26) *r* for solution C cannot be estimated because to our knowledge no data on $\chi$ between deuterated polystyrene and dioctyl phthalate are available.

(27) Adam, M.; Delsanti, M. *J. Phys. (Paris)* **1984**, *45*, 1513.

(28) Saito, S.; Hashimoto, T. *J. Chem. Phys.* **2001**, *114*, 10531.

(29) Tobolsky, A. V. *Properties and Structure of Polymers*; John Wiley & Sons: New York, 1960.

(30) In a strict sense, $\xi \equiv (C/r_0)^{1/2}$ should be determined from the early stage spinodal decompositon of solution A, where *C* is given by eq A7. Our small-angle neutron scattering experiments have revealed that $\xi$ is on the order of 10 nm for a semidilute solution of deuterated polystyrene having the same order of molecular weight and concentration as that under consideration.[4] Thus we employed this value ($\xi$ =10 nm) here to make the calculation as simple as possible. In fact, the choice of $\xi$, if it is reasonable, hardly affects the results of calculation as shown in Figures 3−6, since the excess scattering due to shear appears only at $q < 10^{-3}$ nm$^{-1}$ that is much smaller than $\xi^{-1} = 0.1$ nm$^{-1}$, above which the scattering intensity starts to decrease.

(31) Milner[9] employed a mechanical model that describes the nonlinear viscoelastic behavior with normal stresses, but the calculation of the structure factor was carried out only to the first order of $\dot{\gamma}$. This means normal stresses be zero. Ji et at.[11] employed the Doi−Edwards model derived from the reptation theory with the shear-thinning and normal stresses. However, the calculation of the structure factor was limited at $W_i < 1$, since only one relaxation mode was incorporated.

(32) The intensity can be enhanced only by the convection. The dotted line in Figure 5b denotes the profile obtained by artificially turning off the effect of $\sigma_{xy}$ and $N_1$ on the relaxation rate of the concentration fluctuations (eq 4) (i.e., $(\partial\sigma_{xy}/\partial\phi) = (\partial N_1/\partial\phi) = 0$ in eq 4) at $W_i$ =1.0. In this case, the convective effect is the only factor which affects the concentration fluctuations. The result shows that the intensity is enhanced in the low $q_x$ region to the same level as those with $\partial\sigma_{xy}/\partial\phi \neq 0$. This indicates that in this low $q_x$ region the effects of shear stress and normal stress themselves on $I(q_x)$ almost vanish. Even in the case without the stress−diffusion coupling, the convective effect alone affects the concentration fluctuations having the relaxation rates slower than the shear rate. This enhanced intensity is attributed to the deformation of the fluctuations by the convection: the fluctuations having the relatively long relaxation time compared with the inverse of the shear rate (i.e., the fluctuation in the low *q* region) are deformed and convected before they thermally decays, causing some changes in the intensity distribution (actually, an increase of $S(q_x)$ at small $q_x$'s). The fluctuations having the relatively short relaxation time compared with the inverse of the shear rate (i.e., the fluctuation in the high *q* region) and, on the other hand, decay before they are deformed and convected by shear; hence, no change in the intensity distribution would be observed.

MA0021390